Advanced Composite Materials
Publication details, including instructions for authors and subscription information:
http://www.tandfonline.com/loi/tacm20

On the hot working characteristics of 2124 Al-SiCp metal matrix composites

S. V. S. Narayana Murty , B. Nageswara Rao & B. P. Kashyap

Version of record first published: 02 Apr 2012.

To cite this article: S. V. S. Narayana Murty , B. Nageswara Rao & B. P. Kashyap (2002): On the hot working characteristics of 2124 Al-SiCp metal matrix composites , Advanced Composite Materials, 11:2, 105-120

To link to this article: http://dx.doi.org/10.1163/156855102760410315

Adv. Composite Mater., Vol. 11, No. 2, pp. 105–120 (2002)

Also available online - www.vsppub.com

On the hot working characteristics of 2124 Al–SiC_p metal matrix composites

S. V. S. NARAYANA MURTY [1], B. NAGESWARA RAO [2] and B. P. KASHYAP [3]

[1] *Materials and Metallurgy Group, Vikram Sarabhai Space Centre, Trivandrum 695 022, India*
[2] *Structural Engineering Group, Vikram Sarabhai Space Centre, Trivandrum 695 022, India*
[3] *Department of Metallurgical Engineering and Materials Science, Indian Institute of Technology, Bombay, Mumbai 400 076, India*

Received 19 June 2000; accepted 8 May 2002

Abstract—A simple instability condition is derived following Ziegler's continuum principles for identifying the regions of unstable metal flow during hot deformation in the processing maps. This criterion is examined by considering the flow stress data on 2124 Al–SiC_p metal matrix composites and comparing with the microstructural observations of the deformed compression specimens in the as-vacuum hot pressed condition and vacuum hot pressed and extruded condition. The optimum hot working conditions are proposed from the identified stable regions (having comparatively high values of workability parameters, namely, strain rate sensitivity parameter and efficiency of power dissipation) in the developed processing maps.

Keywords: Efficiency parameter; strain rate sensitivity parameter; instability condition; processing map; 2124 Al–SiC_p metal matrix composites.

1. INTRODUCTION

For aerospace applications, there has been a quest for materials that have high specific strength and toughness. Efforts have been made by researchers to improve the traditional alloys, such as the age hardening Al–Cu–Mg alloy 2024 by reducing the impurities Fe and Si, and designated the new alloy as 2124 [1]. Discontinuously reinforced metal matrix composites, especially particulate reinforced aluminium matrix composites, are currently being used in commercial applications [2–8] because of their high elastic modulus, higher strength and light weight; the ability to economically produce SiC whiskers, platelets and particulates; the ability to use standard shaping methods such as forging, rolling, extrusion, etc.; and much less dependence of the engineering properties on directions than with continuous composites. The hot working parameters for conventional matrix alloys cannot be adopted for these composites due to the presence of hard ceramic reinforcements.

Some enterprises are trading metal-matrix composite (MMC) semi-products, aluminium based, with silicon carbide or alumina as reinforcement, which are produced by casting techniques, such as gravity and discontinuous castings, and which normally have inadequate microstructures and properties, mainly due to porosity and sometimes poor reinforcement wetting. When the final product has a uniform shape, there are several processes for a later thermo-mechanical consolidation (principally hot rolling and extrusion). However, if subsequently non-uniform sections are necessary, then it would be essential to develop some conventional forging process, such as open and closed die forging. A significant problem for MMC forging is the metal matrix stiffness originating from the presence of ceramic particles. This causes an important change in the hot working conditions, provided that the matrix plastic deformation is considerably lowered by the anchoring effect produced by the reinforcement.

Hot workability is concerned with the extent to which a material plastically deforms during shaping at high temperatures without the occurrence of flow localization or fracture. One of the requirements for process modeling is a knowledge of the material flow behavior for defining deformation processing maps that delineate 'safe' and 'nonsafe' hot working conditions. These maps show in the processing space, i.e. on the axes of temperature and strain rate, the processing conditions for stable and unstable deformation.

2124 Al–SiC composites are usually made by a powder metallurgy route, avoiding use of liquid metal, which would produce a brittle reaction zone of Al_4C_3 around the reinforcement. Tuler and Klimowicz [9] have examined the hot working characteristics of 2014 Al and 2219 Al, both reinforced with 15% alumina particulates, as well as the matrix alloys. Flow stress data on metal matrix composites are available for 1100 Al–10 vol% SiC [10], 2024–15 vol% SiC_p [11], 2124 Al–20 vol% SiC [12], 2014 Al–20 vol% Al_2O_3 [13] and 6061 Al–10 vol% Al_2O_3 [14]. Radhakrishna Bhat *et al.* [15] and Prasad and Sasidhara [16] have compiled the flow stress data for 2124 aluminium with varying volume fractions of SiC particulate reinforcements in the vacuum hot pressed and extruded condition. In their studies, the workpiece under hot working conditions is considered to be a dissipator of power. They computed the efficiency of power dissipation (η) from the strain rate sensitivity parameter (m) as,

$$\eta = \frac{2m}{m+1}, \tag{1}$$

and used the instability condition:

$$\xi(\dot{\varepsilon}) = \frac{\delta \ln\left(\frac{m}{m+1}\right)}{\delta \ln \dot{\varepsilon}} + m < 0, \tag{2}$$

for the identification of flow instabilities during hot deformation of materials.

The variation of a dimensionless parameter (η) called the efficiency of power dissipation, with strain (ε), strain rate ($\dot{\varepsilon}$) and temperature (T) constitutes a

processing map. In fact, the efficiency of power dissipation (η) in equation (1) is valid only when the flow stress (σ)–strain rate ($\dot{\varepsilon}$) curve of the material obeys the power law. For complicated alloy systems, the assumption of a power law does not hold good. Hence the instability condition (2) has to be corrected accordingly.

This paper presents briefly the derivation of the flow instability condition applicable for any flow stress–strain rate curve. The potentiality of the derived instability condition has been demonstrated by considering the flow stress data of aluminium alloy 6061 reinforced with 10 vol% alumina and verifying with the reported microstructural observations of the deformed compression specimens [14] as well as the industrial forging trials [17]. A processing map from the flow stress data of AA 2014–20 vol% Al_2O_3 [13] has been generated and verified with the industrial forging trials [18]. Processing maps are also developed by considering the flow stress data on 2124 Al–20 vol% SiC_p in the as-vacuum hot pressed condition [16] and on 2124 aluminum alloy with varying volume fractions of SiC particulate reinforcements in the vacuum hot pressed and extruded condition.

2. ANALYSIS

The total power, P (per unit volume), absorbed by the workpiece material during plastic flow at any strain (ε) and temperature (T) is given by [19, 20],

$$P = G + J, \tag{3}$$

or

$$\sigma\dot{\varepsilon} = \int_0^{\dot{\varepsilon}} \sigma \, \mathrm{d}\dot{\varepsilon} + \int_0^{\sigma} \dot{\varepsilon} \, \mathrm{d}\sigma. \tag{4}$$

The total power, P ($\equiv \sigma\dot{\varepsilon}$) in equation (3) is expressed in terms of two complementary functions, G (the dissipator content) and J (the dissipator co-content), which are defined in equation (4) by the two integrals.

From equation (4), it follows that at any given ε and T, the change in J with respect to G yields the well-known strain rate sensitivity parameter (m) which is,

$$\left(\frac{\partial J}{\partial G}\right)_{\varepsilon,T} = \left[\frac{\partial(\ln\sigma)}{\partial(\ln\dot{\varepsilon})}\right]_{\varepsilon,T} = m. \tag{5}$$

If the flow stress with strain rate at any strain and temperature obeys the power law:

$$\sigma = K\dot{\varepsilon}^m, \tag{6}$$

then,

$$G = \frac{P}{1+m}, \tag{7}$$

$$J = \frac{mP}{1+m}, \tag{8}$$

which can be evaluated directly from P and m. For ideally plastic flow ($m = 1$), the value of J reaches its maximum value,

$$J_{\max} = \frac{1}{2}P. \tag{9}$$

In this case one-half of the power is dissipated in material flow and the other half is dissipated in viscous heat ($G_{\max} = J_{\max} = P/2$). The behaviour of superplastic materials approaches this extreme. The other extreme occurs for materials which are strain rate insensitive, i.e. $m \to 0$. For this case, equations (7) and (8) give $G \to P$ and $J \to 0$. In such a situation all the power would be dissipated by heat, which leads to plastic instability by a continuum process such as adiabatic shearing.

The effect of J on the plastic flow of materials can be visualized if the power dissipation capacity of the work piece is expressed in terms of efficiency of power dissipation, η, which is defined as

$$\eta = \frac{J}{J_{\max}} = \frac{2J}{P}. \tag{10}$$

Substituting the value of J from equation (8) in equation (10), one can obtain the value of η given in equation (1). In general, the workability parameters (m and η) are functions of ε, $\dot{\varepsilon}$ and T. Though the definition of the strain rate sensitivity parameter (m) in equation (5) originates directly from the traditional power law relation (6), when the log–log data from the $\sigma - \dot{\varepsilon}$ plot do not fall on a straight line, m, the slope of the $\log \sigma - \log \dot{\varepsilon}$ curve varies at each point on the curve, and becomes a function of $\dot{\varepsilon}$. At low strain rates, the $\log \sigma - \log \dot{\varepsilon}$ plot represents a straight line, for which the slope m is a constant. Hence, the apparent m values from equation (5) depend on deformation mechanisms in the region for given strain rates and temperatures. For a general flow stress–strain rate curve, the computational procedure for η-evaluation is explained below.

Proper care should be taken while evaluating the integral for J defined in equation (4), which has the limits of integration from zero to σ. This is because the flow stress of the material need not increase monotonically with increasing strain and strain rate. It can have an oscillatory behavior. In such a situation, there is a possibility that the same flow stress will occur at different strains and strain rates. It is better to express the flow stress (σ) in terms of strain (ε), strain rate ($\dot{\varepsilon}$) and temperature (T) for accurate estimation of σ to any specified $\dot{\varepsilon}$ within the interval of the test data using interpolation functions. Hence, the change in the limits of integration is essential in equation (4) for J, from zero to $\dot{\varepsilon}$.

The differential form for the dissipator power co-content, J ($= \int_0^{\sigma} \dot{\varepsilon}\, \mathrm{d}\sigma$) in equation (4) is $\mathrm{d}J = \dot{\varepsilon}\, \mathrm{d}\sigma = \dot{\varepsilon}\frac{\mathrm{d}\sigma}{\mathrm{d}\dot{\varepsilon}}\mathrm{d}\dot{\varepsilon} = \frac{\dot{\varepsilon}}{\sigma}\frac{\mathrm{d}\sigma}{\mathrm{d}\dot{\varepsilon}}\sigma\, \mathrm{d}\dot{\varepsilon} = m\sigma\, \mathrm{d}\dot{\varepsilon}$, which implies that

$$J = \int_0^{\dot{\varepsilon}} m\sigma\, \mathrm{d}\dot{\varepsilon}. \tag{11}$$

J need not be zero when $m = 0$ at any point in the interval of the integration (11). This is because J accounts for the behavior of the material up to $\dot{\varepsilon}$ (global) whereas m gives information at $\dot{\varepsilon}$ (local). Evaluation of the integral (11) requires additional calculations for m. To improve the accuracy in computation, J can be expressed from equations (3) and (4) as

$$J = P - G = \sigma\dot{\varepsilon} - \int_0^{\dot{\varepsilon}} \sigma \, \mathrm{d}\dot{\varepsilon}. \tag{12}$$

The flow stress data are generally reported for $\dot{\varepsilon} > \dot{\varepsilon}_{\min} = 10^{-3}\ \mathrm{s}^{-1}$, whereas the integration for G in equation (12) needs the input from $\dot{\varepsilon} = 0$. To overcome this difficulty, the integral for G is split as

$$G = \int_0^{\dot{\varepsilon}_{\min}} \sigma \, \mathrm{d}\dot{\varepsilon} + \int_{\dot{\varepsilon}_{\min}}^{\dot{\varepsilon}} \sigma \, \mathrm{d}\dot{\varepsilon} = \left[\frac{\sigma\dot{\varepsilon}}{\mathrm{m}+1}\right]_{\dot{\varepsilon}=\dot{\varepsilon}_{\min}} + \int_{\dot{\varepsilon}_{\min}}^{\dot{\varepsilon}} \sigma \, \mathrm{d}\dot{\varepsilon}, \tag{13}$$

and it can be evaluated by numerical quadrature from the test data through a cubic spline fit, which is well established in accuracy. For low strain rates ($< \dot{\varepsilon}_{\min}$), it is assumed that the flow stress (σ)–strain rate ($\dot{\varepsilon}$) curve obeys the power law (6). With this assumption, equation (7) gives the result of the first integral in equation (13). In the absence of flow stress test data for $0 < \dot{\varepsilon} < \dot{\varepsilon}_{\min}$, the value of G computed from equation (13) will have the above limitation. The efficiency of power dissipation (η) can be determined from equations (10)–(13): η variation with ε, $\dot{\varepsilon}$ and T constitutes a three-dimensional processing map, which requires information for delineating regions where fracture or defects are most likely to occur during hot deformation of the material.

The instability condition based on continuum principles for large plastic flows proposed by Ziegler [21] is:

$$\frac{\mathrm{d}D}{\mathrm{d}\dot{\varepsilon}} < \frac{D}{\dot{\varepsilon}}, \tag{14}$$

where D is the dissipation function. In equation (4), the G term represents the power dissipated by plastic work and J is related to the metallurgical mechanisms, which occur dynamically to dissipate power. Metallurgical processes such as dynamic recovery, dynamic recrystallisation, internal fracture (void formation or wedge cracking), dissolution or growth of particles or phases under dynamic conditions, dynamic spheroidization of acicular structures, and deformation induced phase transformation or precipitation under dynamic conditions contribute to the changes in the dissipated power co-content J. Prasad [19] used $D = J$ in his analysis. When $D = J$, equation (14) becomes $\partial J/\partial\dot{\varepsilon} < J/\dot{\varepsilon}$, which implies that

$$\frac{\partial \ln J}{\partial \ln \dot{\varepsilon}} < 1. \tag{15}$$

Assuming the parameter, m, is dependent on $\dot{\varepsilon}$ and using equation (8) for J, the instability condition (2) can be obtained. Strictly speaking, J in equation (8) is

obtained by assuming m as independent of $\dot{\varepsilon}$. If this assumption is true, then the term

$$\frac{\delta \ln\left(\frac{m}{m+1}\right)}{\delta \ln \dot{\varepsilon}}$$

in equation (2) becomes zero, and the instability condition, $\xi = m < 0$. Since the differential form for J in equation (4) as derived earlier, is $\mathrm{d}J = m\sigma \mathrm{d}\dot{\varepsilon}$, the instability condition in equation (15) becomes

$$\frac{\dot{\varepsilon}}{J}\frac{\partial J}{\partial \dot{\varepsilon}} < 1 \Rightarrow \frac{\dot{\varepsilon}}{J} m\sigma < 1 \Rightarrow \frac{P}{J} m < 1. \tag{16}$$

Using equation (10) in equation (16), the instability condition is expressed in terms of η and m as

$$\frac{2m}{\eta} - 1 < 0. \tag{17}$$

The left hand side of equation (17) can be denoted by the instability parameter ξ which, when negative, indicates instability in the material during hot deformation. It can be verified that for a power law nature of the $\sigma - \dot{\varepsilon}$ curve, the efficiency parameter, $\eta = 2m/(m+1)$ gives the value of $\xi = m < 0$ in equation (17). Hence equation (2) becomes erroneous, when m is independent of $\dot{\varepsilon}$.

Hence, the condition for flow instability during hot deformation of material is:

$$\xi = \frac{mP}{J} - 1 = \frac{2m}{\eta} - 1 < 0. \tag{18}$$

The curve $\xi = 0$ bifurcates the stable and unstable regions in the processing maps. The regions in the processing maps where $\xi < 0$ indicate instability in the material during hot deformation. η and m are the important workability parameters to use in equation (18) for delineating unstable regions in the processing maps. These values are determined from the flow stress data of the intended material. A cubic spline fit for the test data is used to generate a greater number of data points for evaluating the integral for G in equation (13) by the trapezoidal rule. After evaluating G, J is obtained from equation (12) by subtracting G from P ($\equiv \sigma\dot{\varepsilon}$). Then the efficiency parameter $\eta = 2J/P$ is determined. While carrying out the numerical computation, the flow stress data is initially transformed into logarithmic scale, in order to reduce the tenth order magnitude of strain rate to first order, to avoid any excessive round-off error. With this transformation, the first derivative of the spline fit gives directly the strain rate sensitivity parameter (m) at the generated intermediate data points. From the values of η and m at the specified values of $\dot{\varepsilon}$ and T, the instability parameter ξ is evaluated. MATLAB (Math Works Inc., US) software was utilised for generating the two-dimensional contour maps on the axes of temperature and strain rate.

3. RESULTS AND DISCUSSION

Initially, the instability condition derived in the preceding section is examined on the flow stress data of 6061 Al–10 vol% Al_2O_3 metal matrix composite [14]. The flow stress data were generated covering the temperature range 350° to 550°C and strain rate range 0.001–100 s^{-1} from compression testing of solid cylinders of size 10 mm in diameter and 15 mm in height using a servo-hydraulic testing machine capable of imposing constant true strain rates on the specimen. Adiabatic temperature rise during high strain rate testing was measured and the flow stress was corrected for the temperature rise. The specimens were compressed to 50% of their initial height and the load–stroke curves obtained in the hot compression were converted in to true stress–true plastic strain curves by subtracting the elastic portion of the strain and using the standard equations for the true stress and true strain calculations. Figure 1 shows the processing map in which unstable regions are identified wherever $\xi < 0$. The microstructural observations of [14] are also marked in Fig. 1 to confirm the validity of the present instability condition (18). The unstable point at $T = 350°C$ and $\dot{\varepsilon} = 0.001$ s^{-1} falls in the stable region of the map (see Fig. 1), which may be due to non-availability of flow stress data for temperatures below 350°C and strain rate below 0.001 s^{-1}. Yeh *et al.* [17] have

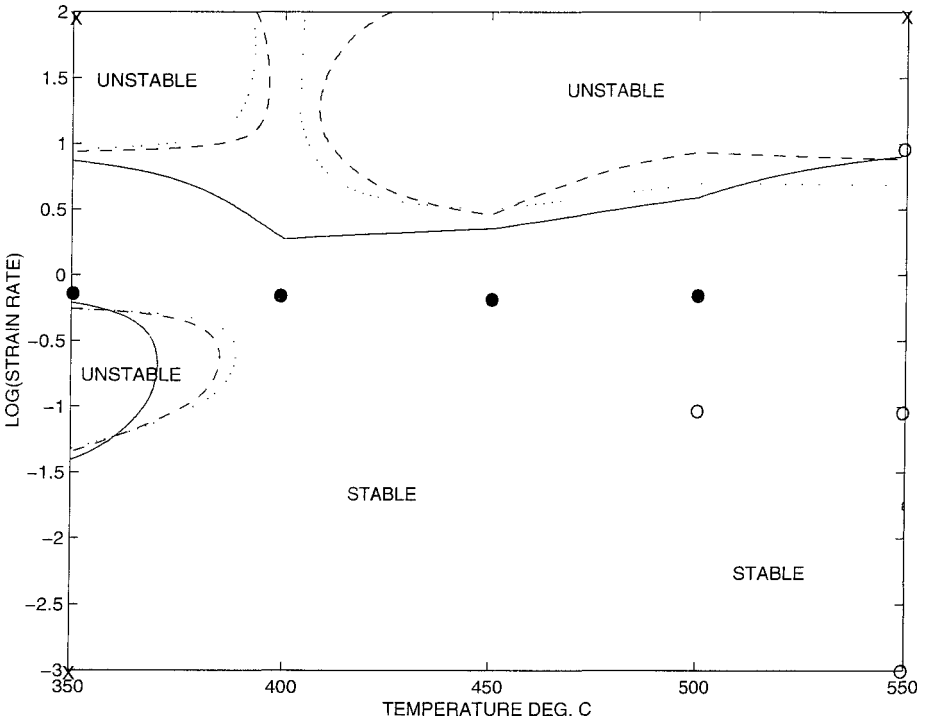

Figure 1. Processing map for 6061 Al–10 vol% Al_2O_3 metal matrix composite at different strains (ε) superimposed; — 0.1; - - - 0.3; and · · · 0.5 with microstructural observations of [14]: (○) stable; (×) unstable and [17] (●) stable.

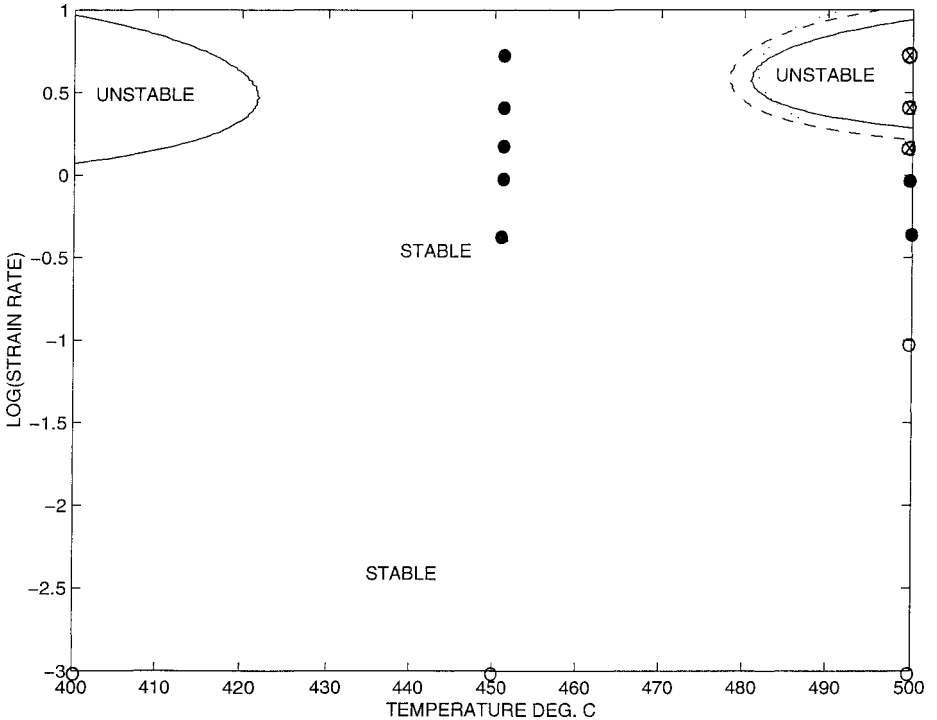

Figure 2. Processing map for 2014 Al–20 vol% Al_2O_3 metal matrix composite at different strains (ε) superimposed; — 0.1; - - - 0.3; and ··· 0.5 with microstructural observations of [13]: (○) stable; and [18]: (●) stable; (⊗) unstable.

conducted forging tests on 6061 Al–10 vol% Al_2O_3 composite in the temperature range 350–500°C with a compressive strain rate of 0.5 s^{-1}. The composite obtained was in the form of 200 mm diameter cast ingots, which were extruded into rods of diameter 22 mm. All the specimens were treated to T6 temper (solution treated at 520°C for 1.5 hours, water quenched, and then aged at 175°C for 8 hours). The average heating rate was about 10°C/s, and the specimens were maintained at the forging temperatures for 3 min before tests. No lubricants between the workpiece and the tools were used during the forging process. After forging, the specimens were cooled in air and then cut along the centerline for metallographic analysis by an optical microscope. No surface cracks were observed in any of the forged specimens in the temperature range of 350–500°C at a strain rate of 0.5 s^{-1}. The processing map also indicates that the temperature range at this strain rate is stable.

Figure 2 shows the processing map for aluminium alloy AA2014–20 vol% Al_2O_3 generated from the flow stress data of [13] and also marked in it are the microstructures of the deformed specimens. It is noted that this composite exhibits a domain of superplasticity at strain rate range of 0.01–0.001 s^{-1} and temperature range of 450–500°C. At higher strain rates (>1 s^{-1}), localized shear bands and cracks were noticed in the deformed specimens. Tezanos *et al.* [18]

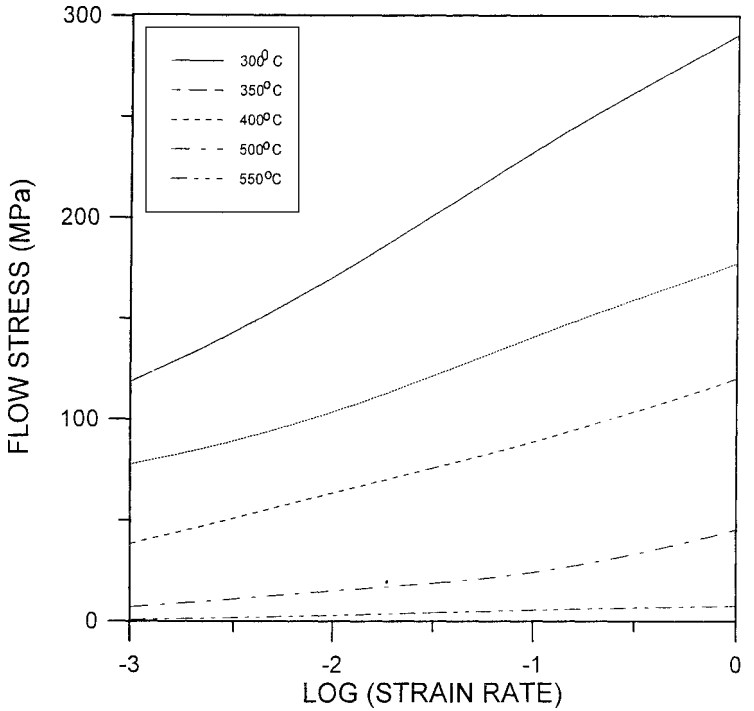

Figure 3. Variation of flow stress with strain rate at different temperatures for $\varepsilon = 0.5$ for 2124 Al–20 vol% SiC particulate reinforced composite in the as-vacuum hot pressed condition.

have examined the hot deformation behaviour of 2014 Al reinforced with 15 vol% Al_2O_3 particulates through forging tests at 430°C and 500°C for the strain rates of 0.5, 1.0, 1.5, 2.5 and 5 s^{-1}. It was noted that the higher the temperature and lower the deformation rate, the easier was the forging. Since the starting material was very porous and had many slag inclusions, a greater number of surface defects were noticed at larger strains and deformation rates. All the microstructures in their recommended forging zone fall in the stable regions of the generated processing map (see Fig. 2) from the flow stress data.

Finally, the instability condition (18) has been applied on the flow stress data [12, 16] of 2124 Al–20 vol% SiC particulate reinforced composite in the as-vacuum hot pressed condition. Figure 3 shows the variation of flow stress with strain rate for a strain of $\varepsilon = 0.5$ and at different temperatures. Figure 4 shows the processing map on which unstable regions are identified under the condition of equation (18) at a strain of 0.3 and 0.5. The microstructural observations reported in [12] are also marked in Fig. 4. The microstructure of the specimen deformed at 550°C and 0.001 s^{-1} corresponding to the peak efficiency showed little difference with the initial microstructure which is expected during superplasticity, since the process involves essentially grain boundary sliding with simultaneous diffusion accommodated flow. This has been attributed to the very fine grain size ($\sim$10 μm)

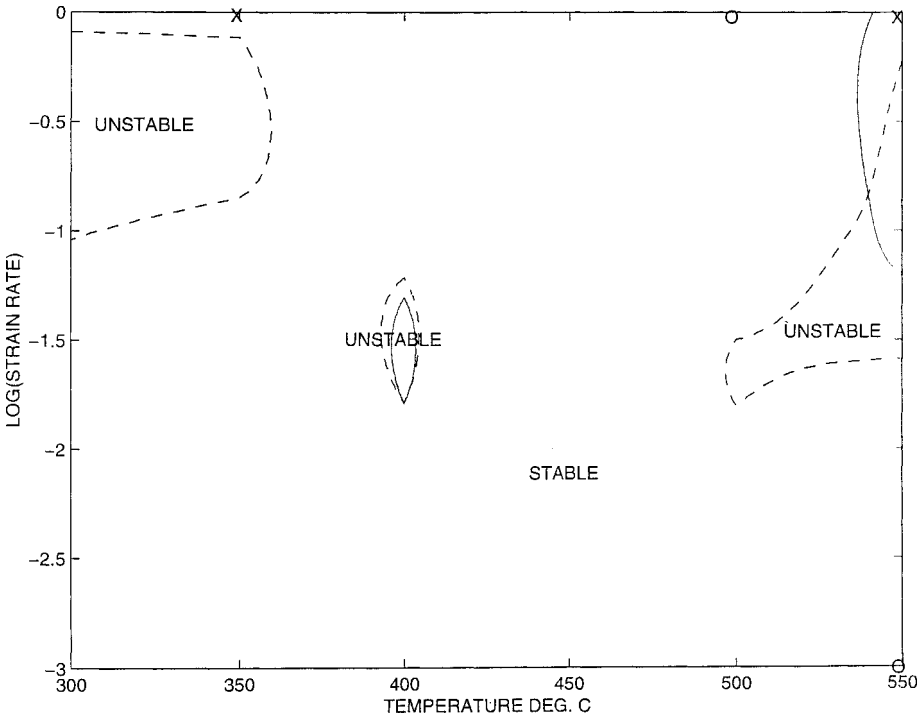

Figure 4. Processing map for 2124 Al–20 vol% SiC_p metal matrix composite in the as-vacuum hot pressed condition at different strains (ε) superimposed; — 0.3 and - - - 0.5 with microstructural observations of [12]: (○) stable; (×) unstable.

of the powder particles along with the absence of grain size variation or cracking at the grain boundaries with deformation. Figures 5 and 6 show the contour map of the efficiency of power dissipation (η) and the strain rate sensitivity parameter (m) at a strain 0.5 respectively. The maximum values of η and m at $\dot{\varepsilon} = 0.001\ s^{-1}$ and $T = 550°C$ are 0.865 and 0.762 respectively. Maximisation of η or m will reduce the tendency for flow localization. The vacuum hot pressed powder compacts have prior particle boundary (PPB) defects which are to be eliminated by hot working to improve ductility. It is desirable to have processing in dynamic recrystallisation (DRX) regime, which reconstitutes the microstructure and redistributes the PPB defects. Hence, it is preferable to have the billet conditioning of the vacuum hot pressed compacts of MMC in the temperature region of 500°C to 525°C at the strain rate of $1\ s^{-1}$ and secondary metal working operations in the superplasticity region ($T = 500°C$ to 550°C and $\dot{\varepsilon} = 0.001$ to $0.01\ s^{-1}$).

Figure 7 shows the processing map for the vacuum hot pressed 2124 Al matrix material at strains of 0.1, 0.3 and 0.5 superimposed onto each other. In the hot deformation of MMC, the matrix phase is very soft compared to the reinforcement and these particulates constrain the matrix flow. Therefore, the flow behaviour of the matrix phase will be modified. The maximum efficiency of the power dissipa-

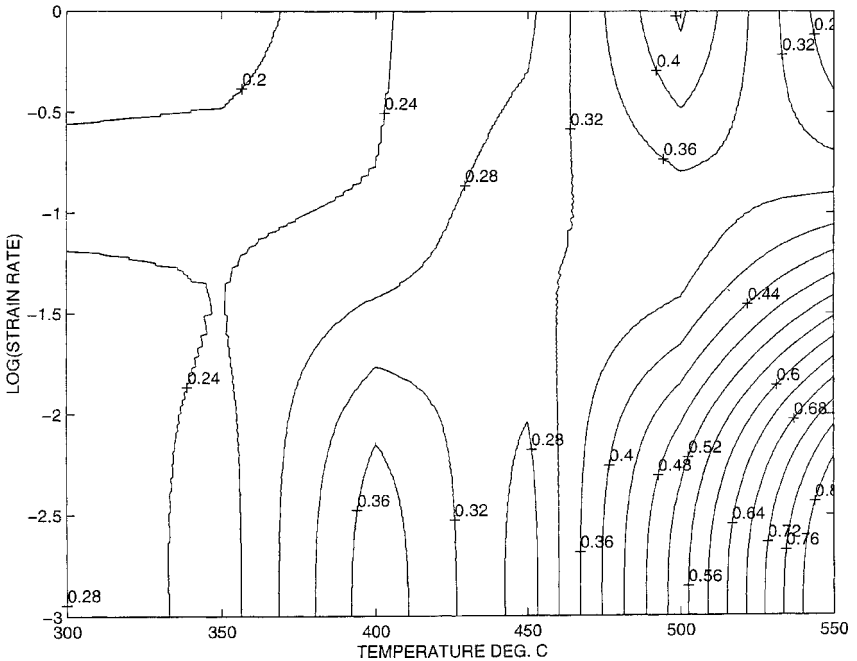

Figure 5. Contour map for the efficiency of power dissipation (η) at a strain (ε) of 0.5 for 2124 Al–20 vol% SiC_p metal matrix composite (vacuum hot pressed condition).

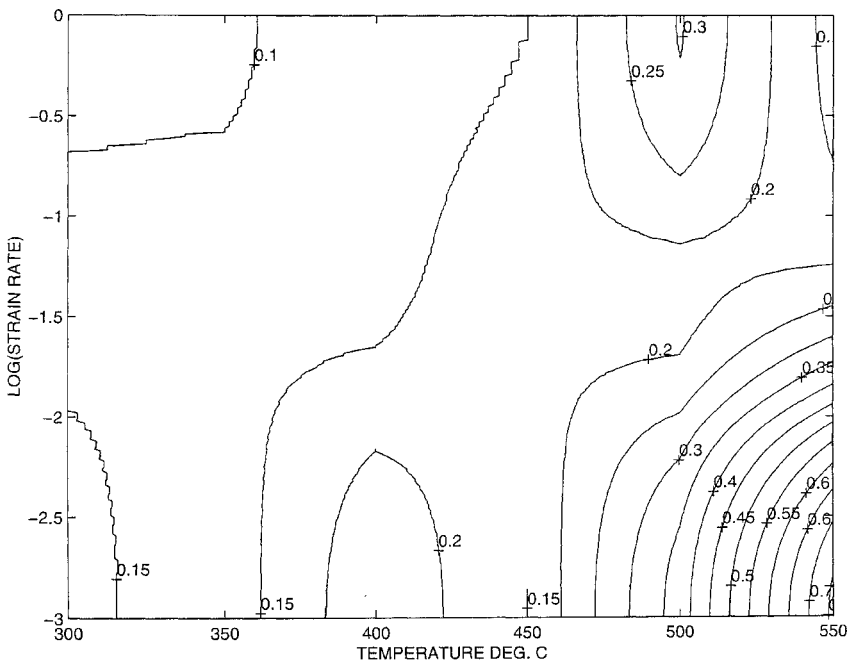

Figure 6. Contour map for the strain rate sensitivity parameter (m) at a strain (ε) of 0.5 for 2124 Al–20 vol% SiC_p metal matrix composite (vacuum hot pressed condition).

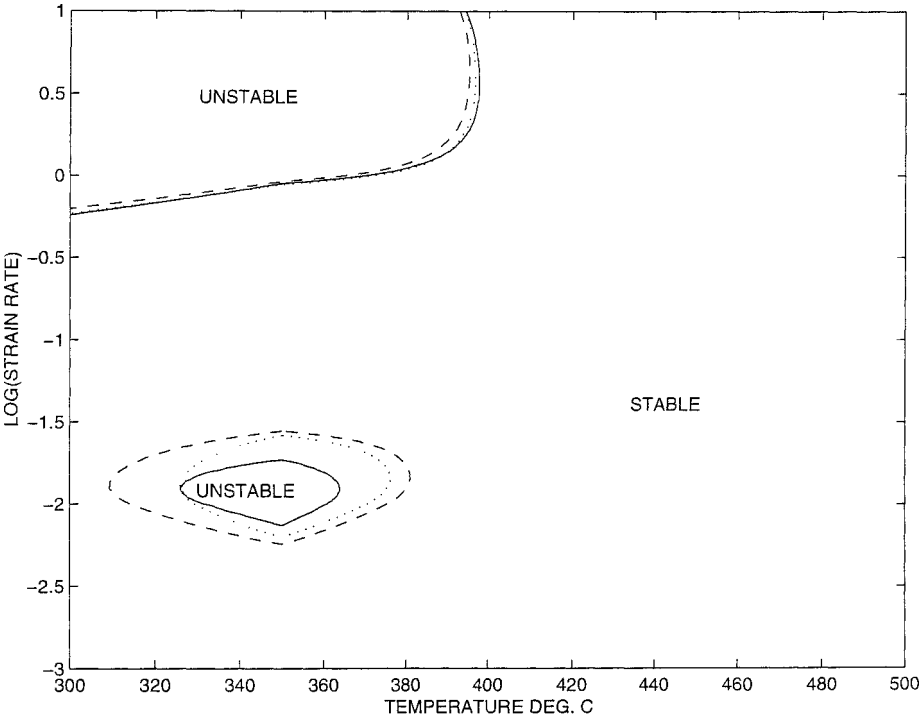

Figure 7. Processing map for 2124 Al in the as-vacuum hot pressed condition at different strains (ε) superimposed; — 0.1; - - - 0.3; and · · · 0.5.

tion in this domain is noted to be 0.431, which is lower than that for the MMC. Microstructural examination of the specimen of the matrix material deformed at 500°C and 0.001 s^{-1} showed dynamic recrystallization with considerable reconstitution of the structure by the elimination of the prior particle boundaries present in the as-hot pressed condition. The microstructure of the MMC deformed at 500°C and 1 s^{-1} exhibited considerable reconstitution of microstructure by dynamically recrystallized grains. The microstructure of the MMC deformed at 300°C and 0.1 s^{-1} exhibited dynamic recovery characterized by a very fine grain size formed by static recrystallization occurring during cooling following dynamic recovery. The microstructure of the MMC deformed at 550°C and 1 s^{-1} shows extensive cracking at PPBs which are the surfaces of the initial surface particles. The microstructure of the MMC deformed at 350°C and 1 s^{-1} revealed flow localization and extensive cracking.

Figures 8–11 show processing maps for 2124 Al with varying volume fractions of SiC particulates, namely, 5, 10, 15 and 20% generated from the flow stress data [16]. It is noted that the domain of instability increases with the volume fraction of the SiC particulates. The maximum value of m and η for all these materials occurs at a temperature of 500°C and a strain rate of 0.001 s^{-1}. This domain represents the process of superplasticity. The matrix material in the as-hot pressed condition does not show any superplasticity domain. The reason for the appearance of the

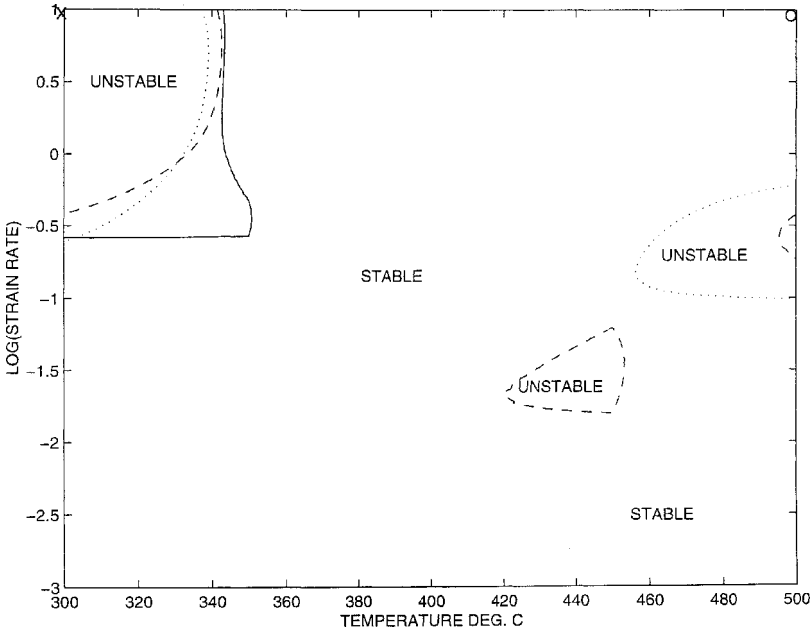

Figure 8. Processing map for 2124 Al–5 vol% SiC_p metal matrix composite (vacuum hot pressed and extruded) at different strains (ε) superimposed; — 0.1; - - - 0.3; and · · · 0.5 with microstructural observations of [16]: (○) stable; (×) unstable.

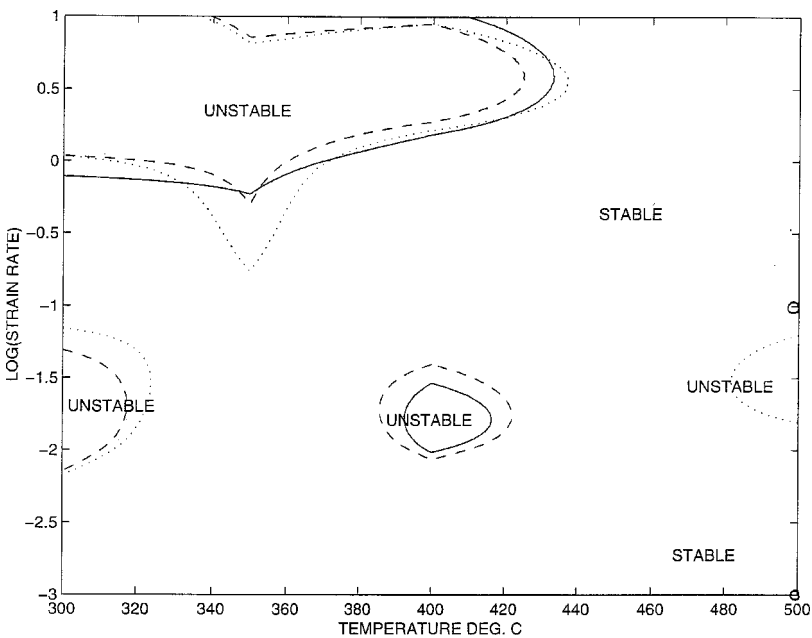

Figure 9. Processing map for 2124 Al–10 vol% SiC_p metal matrix composite (vacuum hot pressed and extruded) at different strains (ε) superimposed; — 0.1; - - - 0.3; and · · · 0.5 with microstructural observations of [15]: (○) stable.

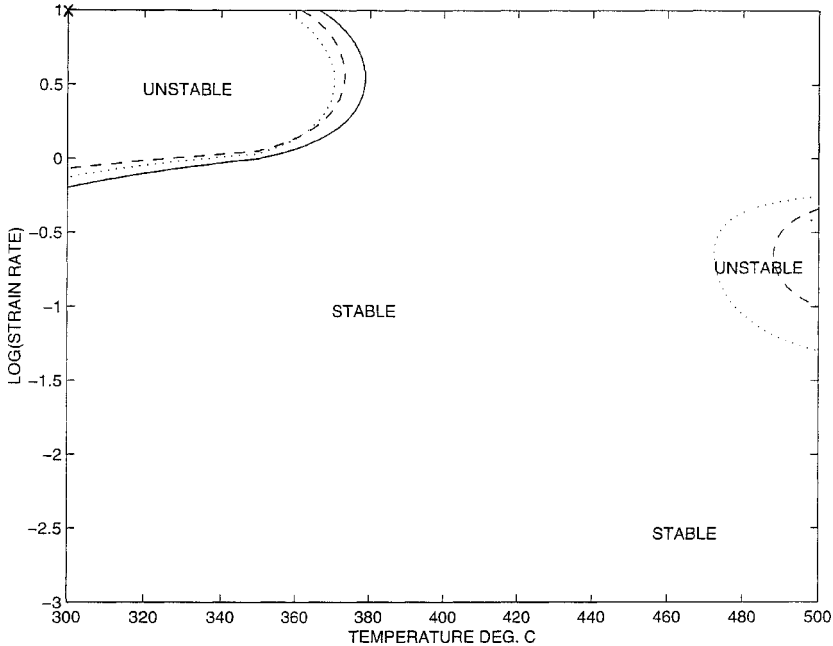

Figure 10. Processing map for 2124 Al–15 vol% SiC_p metal matrix composite (vacuum hot pressed and extruded) at different strains (ε) superimposed; — 0.1; - - - 0.3; and · · · 0.5 with microstructural observations of [15]: (×) unstable.

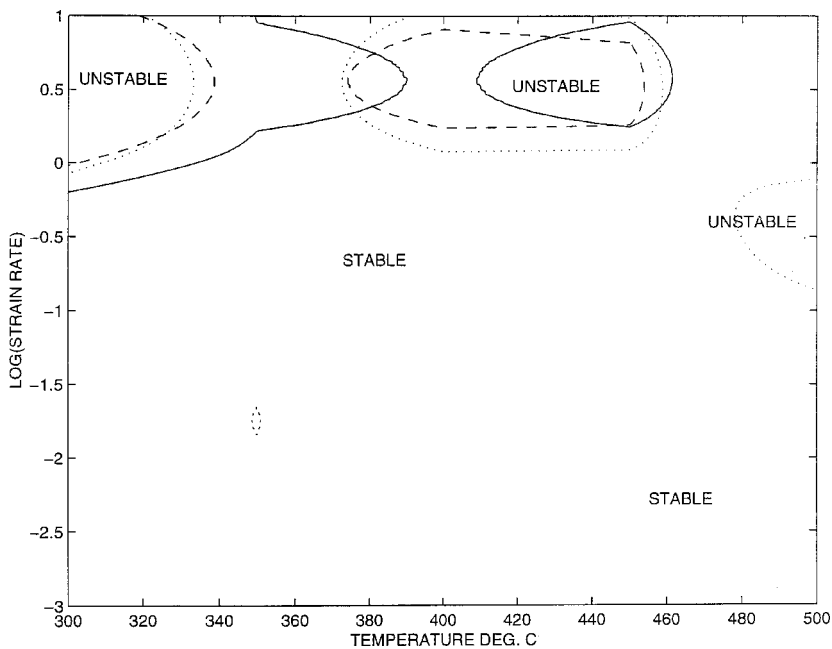

Figure 11. Processing map for 2124 Al–20 vol% SiC_p metal matrix composite (vacuum hot pressed and extruded) at different strains (ε) superimposed; — 0.1; - - - 0.3; and · · · 0.5.

superplasticity domain in the extruded material is the fine grain size produced by recrystallisation after extrusion. The processing maps for 2124 Al–20 vol% SiC_p metal matrix composite in the as-vacuum hot pressed (Fig. 4) and vacuum hot pressed and extruded (Fig. 11) indicate reduction in the instability area in the extruded material as expected.

Stable regions in the processing maps indicate that a volume fraction of 15% is ideal for superplasticity, keeping the other variables such as particle size, matrix materials and reinforcement type unchanged. In industrial practice, highest possible strain rates and lowest possible flow stresses are preferred from a productivity viewpoint. Hence, it is preferable to have the billet conditioning of the 2124 aluminium metal matrix composites in the temperature region of 450°C to 500°C and in the strain rate range of 1 to 10 s^{-1} and secondary metal working operations in the superplasticity region ($T = 450$°C to 500°C and $\dot{\varepsilon} = 0.001$ to 0.01 s^{-1}).

4. CONCLUSIONS

A simple instability condition derived for any flow stress – strain rate curve has been applied for identifying the regimes of instabilities in the processing maps during hot deformation of 2124 Al–20 vol% SiC particulate metal matrix composite in the as vacuum hot pressed condition. The instability condition is verified with the microstructural observations of the deformed specimens. The hot deformation characteristics of 2124 aluminium with varying volume fractions of SiC reinforcements in the vacuum hot pressed and extruded condition have been examined. The optimum hot working conditions for these materials are suggested from the processing maps in the stable regions where the workability parameters are relatively maximum. All the alloys studied here exhibit two domains: one at high strain rates and another at low strain rates. The high strain rate domain can be used for bulk processing whereas the lower strain rate domain is preferable for secondary processing, like superplastic forming. From the flow stress data, the boundaries in the processing maps are drawn between the stable and unstable regions by utilising the instability condition, equation (18), which is based on Ziegler's continuum principles. Uncertainties (if any) on the boundaries between the 'stable' and 'unstable' regions in the processing maps, will be due mainly to the flow stress data. To define the processing windows in the desired range of strain rates, workability parameters in the stable regions should be relatively maximum in the selected temperature domain.

REFERENCES

1. T. S. Srivastan, D. Lanning, Jr. and K. K. Soni, Microstructure, tensile properties and fracture behaviour of an Al-Cu-Mg alloy 2124, *J. Mater. Sci.* **28**, 3205–3213 (1993).
2. D. J. Lloyd, Particle reinforced aluminium and magnesium matrix composites, *Int. Mater. Rev.* **39**, 1–23 (1994).
3. H. R. Sherdiff and M. F. Ashby, Design with metal matrix composites, *Mater. Sci. Technol.* **10**, 443–451 (1994).

4. I. Sinclair and P. J. Gregson, Structural performance of discontinuous metal matrix composites, *Mater. Sci. Technol.* **13**, 709–726 (1997).
5. A. P. Divecha, S. G. Fishman and S. D. Karmarkar, Silicon carbide reinforced aluminium-A formable composite, *J. Metals* **9**, 2–17 (1981).
6. R. J. Arsenault, The strengthening of aluminium alloy 6061 by fiber and platelet silicon carbide, *Mater. Sci. Engng. A* **64**, 171–181 (1984).
7. H. J. Rack, Powder techniques in processing of metal matrix composites, in: *Metal Matrix Composites-Processing and Interfaces*, R. K. Everlett and R. J. Arsenault (Eds), pp. 83–100. Academic Press (1991).
8. D. L. McDanels, Analysis of stress–strain, fracture and ductility behaviour of aluminium matrix composites containing discontinuous silicon carbide reinforcement, *Metal. Trans A* **16**, 1105–1115 (1985).
9. F. R. Tuler and T. F. Klimowicz, Deformation processing of Alumina–Aluminum metal matrix composites, in: *Metal and Ceramic Composites: Processing, Modeling and Mechanical Behaviour*, R. B. Bhagat, A. H. Clauer, P. Kumar and A. M. Ritter (Eds), pp. 271–280. TMS, Warrandale, PA (1990).
10. B. V. Radhakrishna Bhat, Y. R. Mahajan, H. Md. Roshan and Y. V. R. K. Prasad, Processing maps for hot working of powder metallurgy 1100 Al–10 vol% SiC particle metal matrix composite, *J. Mater. Sci.* **28**, 2141–2147 (1993).
11. B.-C. Ko and Y.-C. Yoo, Prediction of dynamic recrystallization condition by deformation efficiency for Al 2024 composite reinforced with SiC particles, *J. Mater. Sci.* **35**, 4073–4077 (2000).
12. B. V. Radhakrishna Bhat, Y. R. Mahajan, H. Md. Roshan and Y. V. R. K. Prasad, Processing map for hot working of powder metallurgy 2124 Al-20% SiC_p metal matrix composite, *Metal. Trans A* **23**, 2223–2230 (1992).
13. B. V. Radhakrishna Bhat, Y. R. Mahajan, H. Md. Roshan and Y. V. R. K. Prasad, Characteristics of superplasticity domain in the processing map for hot working of an Al alloy 2014–20 vol% Al_2O_3 metal matrix composite, *Mater. Sci. Engng A* **189**, 137–145 (1994).
14. B. V. Radhakrishna Bhat, Y. R. Mahajan, H. Md. Roshan and Y. V. R. K. Prasad, Processing map for hot working of 6061 Al–10 vol% Al_2O_3 metal matrix composite, *Mater. Sci. Technol.* **11**, 167–173 (1995).
15. B. V. Radhakrishna Bhat, Y. R. Mahajan, H. Md. Roshan and Y. V. R. K. Prasad, Effect of volume fraction of SiCp reinforcement on the processing maps for 2124 Al matrix composites, *Metal. Mater. Trans A* **31**, 629–639 (2000).
16. Y. V. R. K. Prasad and S. Sasidhara: *Hot Working Guide — A Compendium of Processing Maps*, ASM, Metals Park, OH, USA (1997).
17. M. S. Yeh, W. P. Weng, S. C. Wang and T. H. Chuang, Plastic flow behaviour during the forging of a 6061 Al–10 vol% $Al_2O_{3(P)}$ composite, *Metal. Mater. Trans. A* **31A**, 1310–1313 (2000).
18. F. J. Tezanos, J. Goni, A. Fernandez and C. Foruria, Forging process of metal matrix composites reinforced with particles, in: *Proceedings of the 9th International Conference on Composite Materials (IICM-9)*, Madrid (1993), Antonio Miravete (Ed.), pp. 869–876. University of Zaragoza and Woodhead Publishing Limited, Zaragoza, Spain (1993).
19. Y. V. R. K. Prasad, Recent advances in the science of mechanical processing, *Indian J. Technol.* **28**, 435–451 (1990).
20. Y. V. R. K. Prasad and T. Seshacharyulu, Modeling of hot deformation for microstructural control, *Int. Mater. Rev.* **44**, 243–258 (1998).
21. H. Ziegler, Some extremum principles in irreversible thermodynamics, with application to continuum mechanics, in: *Progress in Solid Mechanics*, Vol. 4, pp. 93–193. John Wiley, New York, USA (1963).